

Immiscible and miscible states in binary condensates in the ring geometry

Zhaopin Chen¹, Yongyao Li^{1,2}, Nikolaos P. Proukakis³, and Boris A. Malomed¹

¹*Department of Physical Electronics, School of Electrical Engineering,
Faculty of Engineering, Tel Aviv University, Tel Aviv 69978, Israel*

²*School of Physics and Optoelectronic Engineering, Foshan University, Foshan 52800, China*

³*Joint Quantum Centre (JQC) Durham-Newcastle,
School of Mathematicss, Statistics and Physics, Newcastle University,
Newcastle upon Tyne NE1 7RU, England, United Kingdom*

We report detailed investigation of the existence and stability of mixed and demixed modes in binary atomic Bose-Einstein condensates with repulsive interactions in a ring-trap geometry. The stability of such states is examined through eigenvalue spectra for small perturbations, produced by the Bogoliubov-de Gennes equations, and directly verified by simulations based on the coupled Gross-Pitaevskii equations, varying inter- and intra-species scattering lengths so as to probe the entire range of miscibility-immiscibility transitions. In the limit of the one-dimensional (1D) ring, i.e., a very narrow one, stability of mixed states is studied analytically, including hidden-vorticity (HV) modes, i.e., those with opposite vorticities of the two components and zero total angular momentum. The consideration of demixed 1D states reveals, in addition to stable composite single-peak structures, double- and triple-peak ones, above a certain particle-number threshold. In the 2D annular geometry, stable demixed states exist both in radial and azimuthal configurations. We find that stable radially-demixed states can carry arbitrary vorticity and, counter-intuitively, the increase of the vorticity enhances stability of such states, while unstable ones evolve into randomly oscillating angular demixed modes. The consideration of HV states in the 2D geometry expands the stability range of radially-demixed states.

I. INTRODUCTION

Superfluid mixtures are currently routinely probed in experiments with ultracold atomic gases. In addition to Bose-Bose mixtures of different isotopes and atomic species [1–18], experimentalists have in the past few years created condensates with a spin degree of freedom [19], also implementing spin-orbit coupling which gives rise to exciting new states [20–24]; moreover, recent achievements have led to the generation of doubly-superfluid Bose-Fermi mixtures [25], in which both components are condensed, a state so far inaccessible in other settings (such as superfluid helium). Although the stability and phase diagrams of such systems have been extensively studied in the course of more than 20 years [26–51], even simple hetero-species binary mixtures still reveal unexpected features, such as the role of the trap sag, atom number and kinetic energy contribution to the extent of miscibility in trapped configurations [42, 50], and nontrivial effects of the expansion on the mixtures' dynamics [51, 52].

Configurations which keep drawing growing interest in studies of ultracold atomic gases are based on the annular, alias ring-trap, geometry [53–59]. These configurations are interesting as they lead to closed geometries with controlled flows, that are also of potential use to the emerging field of atomtronics [57, 60]. In this context, mixtures of atomic condensates in toroidal traps and the possibility of sustaining stable persistent currents in them have been previously considered in [61–70], and the corresponding experimental observation [71] has helped to clarify some issues, also raising new questions, such as expansion of the stability area for such states. The aim of the present work is to perform a full classification of accessible stable mixture states in such a geometry, including examination of their stability and decay channels of their unstable counterparts, both in the absence and presence of overall rotation. Given the potential significance of multi-component states in ring-shaped traps for applications such as rotational sensors, such a classification is relevant. It can also assist in developing methods for control of such mixtures in the experimental work which is currently going on in many laboratories.

Specifically, in this work, we construct a binary Bose-Einstein-condensate (BEC) system trapped in an annular geometry, through the mean-field analysis in the presence of inter- and intra-species interactions, whose parameters are varied in broad limits. After analyzing the corresponding one-dimensional (1D) problem, we focus on the more experimentally-relevant 2D annular structure. We implement periodic boundary conditions (b.c.) in the azimuthal direction in the 1D case, and zero b.c. at inner and outer boundaries of the 2D annular structure. The latter b.c. set enables one to study how the annular structure affects density patterns in the repulsive bosonic mixtures, as a result of the existence of different demixed and mixed states, and their stability.

This paper is structured as follows. First, Sec. II introduces and analytically considers our basic model for the mixtures in both 1D and 2D geometries, and presents analytical results for spatially uniform 1D mixed solutions, with zero and hidden vorticities (HV), the latter implying opposite topological charges in the two components, which makes it possible to construct stable binary vortex states with zero total angular momentum in nonlinear optics

[72–76] and BEC [52, 77–83]. Most essential are analytical results for stability of these states. Sec. III presents the key results, showing various types of mixed and demixed states in 1D, characterized by different numbers of peaks in them, and both mixed and demixed 2D states. The latter ones include both radially-demixed modes, with different vorticities, and their azimuthally-demixed counterparts. Such states are obtained by means of the imaginary-time-propagation method, applied to the coupled Gross-Pitaevskii equations (GPEs). We also address effects of the strength of the repulsive intra-component interaction, annular width, and embedded vorticity on the existence and stability of different states. A noteworthy finding is that the stable radially-demixed states can exist with arbitrary vorticity. Our findings are summarized in Sec. IV.

II. THE MEAN-FIELD MODELS

At low temperatures, a binary condensate mixture is well described by the mean-field theory for the set of wave functions ϕ and ψ of the two components. Here we address the system (e.g., a heteronuclear one) which does not admit linear interconversion (Rabi and/or spin-orbit coupling) between the components. The wave functions obey the system of GPEs with nonlinear terms accounting for self- (intra-species) and cross- (inter-species) interactions. In the normalized form, the GPE system is written as

$$i\phi_t + \frac{1}{2m_1}\nabla^2\phi - \left(g_1|\phi|^2 + g_{12}|\psi|^2\right)\phi = 0, \quad (1)$$

$$i\psi_t + \frac{1}{2m_2}\nabla^2\psi - \left(g_2|\psi|^2 + g_{12}|\phi|^2\right)\psi = 0,$$

where $m_{1,2}$ are scaled atomic masses, $g_{1,2}$ are coefficients of self-interaction in species ϕ and ψ , and $g_{12} > 0$ is the cross-interaction coefficient. In this work, the analysis is restricted to repulsive interactions, with $g_{1,2,12} > 0$. Then, condition $g_{12} = \sqrt{g_1 g_2}$ separates the mixing ($\sqrt{g_1 g_2} > g_{12}$) and phase-separation (demixing, $\sqrt{g_1 g_2} < g_{12}$) regimes in free space [84]. This criterion is modified by the presence of a trapping potential, which tends to enhance the miscibility [42, 50, 85].

Equations (1) are supplemented by b.c. set at rigid edges, $r = r_{\text{outer}}$ and $r = r_{\text{inner}}$ of the annular area filled by the condensate (r is the radial coordinate):

$$\phi(r = r_{\text{outer,inner}}) = \psi(r = r_{\text{outer,inner}}) = 0. \quad (2)$$

By means of scaling, we fix

$$r_{\text{inner}} \equiv 1, \quad (3)$$

and define the annulus' width,

$$w \equiv r_{\text{outer}} - 1. \quad (4)$$

These b.c. imply that the annular area is confined by rigid circular potential walls, as in a recent experiment [86] (performed for a gas of fermions).

The total norm of the 2D system is

$$N = \int \int (|\phi|^2 + |\psi|^2) dx dy \equiv N_\phi + N_\psi, \quad (5)$$

where the integration is performed over the annular region, or over the circumference, in the 1D limit, which corresponds to very tight confinement in the radial direction [see Eq. (33)] below. The energy (Hamiltonian) of the coupled system is

$$E = \int \int \left[\frac{1}{2m_1} |\nabla\phi|^2 + \frac{1}{2m_2} |\nabla\psi|^2 + \frac{1}{2} (g_1|\phi|^4 + g_2|\psi|^4) + g_{12}|\phi|^2|\psi|^2 \right] dx dy, \quad (6)$$

which is accordingly reduced in the 1D limit.

A. The one-dimensional setting

To define the 1D limit, we assume that the single coordinate, x , running along the ring of radius $r = 1$ [which is fixed by scaling in agreement with Eq. (3)], takes values $0 \leq x \leq 2\pi$. Then, the substitution of solutions in the Madelung form,

$$\phi(x, t) = a(x, t) \exp(i\chi(x, t)) \quad , \quad \psi(x, t) = b(x, t) \exp(i\eta(x, t)) \quad , \quad (7)$$

leads to the system of four real equations for the amplitudes and phases:

$$a_t + \frac{1}{2m_1} a \chi_{xx} + \frac{1}{m_1} a_x \chi_x = 0, \quad (8)$$

$$b_t + \frac{1}{2m_2} b \eta_{xx} + \frac{1}{m_2} b_x \eta_x = 0, \quad (9)$$

$$-a \chi_t + \frac{1}{2m_1} a_{xx} - \frac{1}{2m_1} a \chi_x^2 - g_1 a^3 - g_{12} b^2 a = 0, \quad (10)$$

$$-b \eta_t + \frac{1}{2m_2} b_{xx} - \frac{1}{2m_2} b \eta_x^2 - g_2 b^3 - g_{12} a^2 b = 0. \quad (11)$$

1. The analytical approach in the 1D case

Choosing the constant amplitudes of the two states as a_0 and b_0 respectively, we obtain CW (continuous-wave) solutions of the HV type of Eqs. (8)-(11),

$$\chi = -\mu_1 t + sx \quad , \quad \eta = -\mu_2 t - sx, \quad (12)$$

$$\mu_1 = g_1 a_0^2 + g_{12} b_0^2 + (s^2/2m_1) \quad , \quad \mu_2 = g_2 b_0^2 + g_{12} a_0^2 + (s^2/2m_2) . \quad (13)$$

Here integer s determines the opposite vorticities in the two components, without introducing net phase circulation. To address the important issue of the stability of the HV-CW state, or the zero-vorticity one in the case of $s = 0$, perturbed solutions to Eqs. (8)-(11) are looked for as

$$\begin{aligned} a(x, t) &= a_0 + \delta a \exp(\sigma t + ipx) , \\ b(x, t) &= b_0 + \delta b \exp(\sigma t + ipx) , \end{aligned} \quad (14)$$

$$\begin{aligned} \chi(x, t) &= -\mu_1 t + sx + \delta \chi \exp(\sigma t + ipx) , \\ \eta(x, t) &= -\mu_2 t - sx + \delta \eta \exp(\sigma t + ipx) , \end{aligned}$$

where σ is the instability growth rate (which may be complex), p is a real wavenumber of the perturbations, while $\delta a, \delta b$ and $\delta \chi, \delta \eta$ are their infinitely small amplitudes. The substitution of these expressions in Eqs. (8) - (11) and linearization [i.e., the derivation of the respective Bogoliubov - de Gennes (BdG) equations] yields the following dispersion equation for $\sigma(p)$:

$$\begin{vmatrix} \sigma + i \frac{s}{m_1} p & 0 & -\frac{p^2}{2m_1} & 0 \\ 0 & \sigma - i \frac{s}{m_1} p & 0 & -\frac{p^2}{2m_2} \\ -\frac{p^2}{2m_1} - 2g_1 a_0^2 & -2g_{12} a_0 b_0 & -\sigma - i \frac{s}{m_1} p & 0 \\ -2g_{12} a_0 b_0 & -\frac{p^2}{2m_2} - 2g_2 b_0^2 & 0 & -\sigma + i \frac{s}{m_2} p \end{vmatrix} = 0. \quad (15)$$

Next, we consider two separate cases, depending on the value of s .

2. Zero-vorticity states, $s = 0$

For $s = 0$, determinant (15) defining the stability takes the explicit form

$$\begin{aligned} p^8 + 4(g_1 a_0^2 m_1 + g_2 b_0^2 m_2) p^6 + 4[\sigma^2 m_1^2 + \sigma^2 m_2^2 - 4a_0^2 b_0^2 m_1 m_2 (g_{12}^2 - g_1 g_2)] p^4 \\ + 16(g_1 a_0^2 m_2 + g_2 b_0^2 m_1) m_1 m_2 \sigma^2 p^2 + 16\sigma^4 m_1^2 m_2^2 = 0. \end{aligned} \quad (16)$$

Due to the periodic b.c. set by the ring geometry, p is quantized,

$$p = n/r, \quad n = 0, \pm 1, \pm 2, \dots \quad (17)$$

(recall we here fix $r = 1$ by means of scaling). The onset of the transition to the immiscibility (i.e., instability against the phase separation) is signalled by condition $\sigma(p = \pm 1/r) = 0$. It follows from Eq. (16) that this instability takes place at

$$g_{12}^2 - g_1 g_2 > (g_{12}^2 - g_1 g_2)_{\text{cr}} \equiv \frac{r^{-2} [4(m_1 g_1 a_0^2 + m_2 g_2 b_0^2) + r^{-2}]}{16 m_1 m_2 a_0^2 b_0^2}. \quad (18)$$

Note that even in the case of $g_1 = g_2 = 0$ (no self-repulsion), Eq. (18) yields a finite threshold for the onset of the phase-separation instability:

$$(g_{12}^2 - g_1 g_2)_{\text{cr}}|_{g_1=g_2=0} = \frac{r^{-4}}{16 m_1 m_2 a_0^2 b_0^2}. \quad (19)$$

This result explicitly demonstrates that periodic b.c. provide for partial stabilization of the mixed state, in comparison with the infinite free space, cf. Ref. [84].

3. Hidden-vorticity (HV) states, $s \geq 1$

As defined above, HV states carry opposite angular momenta in the two components of the mixture, while the total momentum is zero. In an explicit form, the corresponding equation (15), which determines their stability, takes a very cumbersome form. It becomes relatively simple in the case of full symmetry in Eqs. (8)-(11) and (12)-(13), *viz.*,

$$m_1 = m_2 \equiv m, \quad g_1 = g_2 \equiv g, \quad g_{12} \equiv 1, \quad a_0 = b_0, \quad (20)$$

for which we obtain $\mu_1 = \mu_2 = -(g+1)a_0^2 + s^2/(2m)$. Then, Eq. (15) can be explicitly written as

$$16m^4 \sigma^4 + (32s^2 + 32gma_0^2 + 8p^2) m^2 p^2 \sigma^2 + 16 \left[(gma_0^2 - s^2)^2 - m^2 a_0^4 \right] p^4 + 8(gma_0^2 - s^2) p^6 + p^8 = 0. \quad (21)$$

Alternatively, the free term in Eq. (21) (the part which does not contain σ^2) can be written as

$$16 \left[(gma_0^2 - s^2)^2 - m^2 a_0^4 \right] p^4 + 8(gma_0^2 - s^2) p^6 + p^8 \equiv [4(gma_0^2 - s^2) + p^4]^2 - 16m^2 a_0^4 p^4.$$

Further, Eq. (21) can be cast in the rescaled form,

$$16\Sigma^2 + 8(4\gamma + 4g + P)P\Sigma + 16 \left[(g - \gamma)^2 - 1 \right] P^2 + 8(g - \gamma)P^3 + P^4 = 0. \quad (22)$$

with

$$\Sigma \equiv \sigma^2/a_0^4, \quad P \equiv p^2/(ma_0^2), \quad (23)$$

which implies measuring σ^2 and p^2 in their natural units, and demonstrates that the equation depends on two parameters only,

$$\gamma \equiv s^2/(ma_0^2) \quad \text{and} \quad g. \quad (24)$$

Typical examples of the $\Sigma(P)$ dependence for unstable and stable HV states, produced by Eq. (22), are presented in Figs.1(a) and (b), respectively. Note that the underlying quantization condition (17) implies that P takes, in fact, only discrete values:

$$P_n = \frac{n^2}{ma_0^2 r^2}, \quad b = 0, 1, 2, \dots \quad (25)$$

The stability condition means that, for all discrete values of P , given by Eq. (25), Eq. (22) must produce negative real solutions for Σ . Full consideration of the stability conditions following from Eq. (22) is too cumbersome for the analytical investigation. Nevertheless, for the infinite system [$r \rightarrow \infty$, i.e., considering P as a continuous variable,

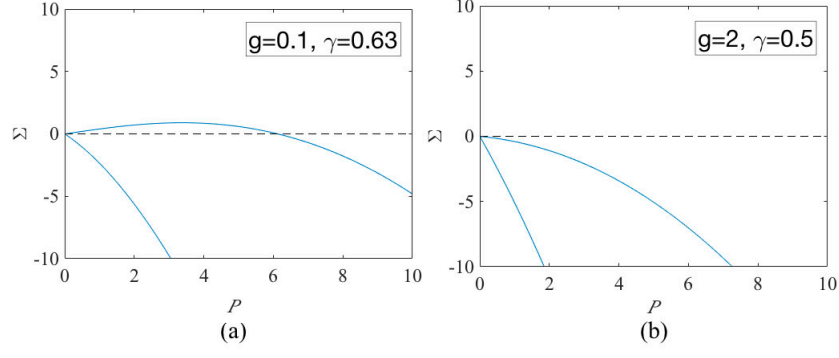


FIG. 1: (Color online) (a) and (b): Eigenvalues produced by Eq. (22) for unstable and stable 1D HV (hidden-vorticity) modes, respectively. The parameters are $(g, \gamma) = (0.1, 0.63)$ in (a), and $(g, \gamma) = (2, 0.5)$ in (b). Positive values of Σ imply, according to its definition (23), the existence of an unstable eigenvalue, $\sigma = \pm a_0^2 \sqrt{\Sigma}$. Panel (a) shows that Σ vanishes at $P = 0$ and $P = 6.12$, as predicted by Eq. (28).

rather than the discrete one, defined by Eq. (25)], it is easy to obtain the stability condition in the limit of $P \rightarrow 0$, for which Eq. (22) amounts to

$$16\Sigma^2 + 8(4\gamma + 4g)P\Sigma + 16[(g - \gamma)^2 - 1]P^2 = 0. \quad (26)$$

It is easy to see that Eq. (26) produces stable solutions, i.e., real $\Sigma < 0$ [see Eqs. (14) and (23)], under condition $|g - \gamma| \geq 1$, i.e., in either of the two cases:

$$g \geq 1 + \gamma, \text{ or } \gamma \geq 1 + g. \quad (27)$$

According to Eq. (24), conditions (27) hold in the case of a relatively high nonlinearity (large g , or the atom number), or large hidden vorticity, s^2 , which appears in Eq. (24), see further details below.

Further, it is possible to find values of P at which Σ vanishes: substituting $\Sigma = 0$ in Eq. (22), one obtains

$$P = 0 \text{ and } P = 4(\gamma - g \pm 1). \quad (28)$$

If Eq. (28) yields $P \leq 0$, i.e., $g \geq 1 + \gamma$, cf. Eq. (27), this implies that the HV states are *completely stable* both for the infinite system and the ring (since, by definition, P may only be positive).

Note the modulational stability of uniform HV states with periodic boundary conditions was studied in Ref. [78] for the case of the attractive nonlinearity (on the contrary to the repulsive nonlinearity considered here), for which it was found that the HV-CW states can *never* be stable.

B. The two-dimensional setting

Stationary solutions to Eq. (1) are looked for in the general form:

$$\phi(r, \theta, t) = \Phi_S(r) \exp(-i\mu_1 t + iS_1 \theta), \quad \psi(r, \theta, t) = \Psi_S(r) \exp(-i\mu_2 t + iS_2 \theta), \quad (29)$$

where (r, θ) are the polar coordinates, $\mu_{1,2}$ chemical potentials of the two components, $S_{1,2} = 0, 1, 2, \dots$ their vorticities [87], and real wave functions Φ and Ψ obey the radial equations:

$$\begin{aligned} \mu_1 \Phi_S + \frac{1}{2m_1} \left(\frac{d^2}{dr^2} + \frac{1}{r} \frac{d}{dr} - \frac{S_1^2}{r^2} \right) \Phi_S - \left(g_1 |\Phi_S|^2 + g_{12} |\Psi_S|^2 \right) \Phi_S &= 0, \\ \mu_2 \Psi_S + \frac{1}{2m_2} \left(\frac{d^2}{dr^2} + \frac{1}{r} \frac{d}{dr} - \frac{S_2^2}{r^2} \right) \Psi_S - \left(g_2 |\Psi_S|^2 + g_{12} |\Phi_S|^2 \right) \Psi_S &= 0, \end{aligned} \quad (30)$$

To address its stability, we replace the stationary solutions with perturbed ones:

$$\begin{aligned}\phi(r, \theta, t) &= \left(\Phi(r) + u_1 e^{\sigma t + i l \theta} + u_2^* e^{\sigma^* t - i l \theta} \right) e^{-i \mu_1 t + i S_1 \theta}, \\ \psi(r, \theta, t) &= \left(\Psi(r) + v_1 e^{\sigma t + i l \theta} + v_2^* e^{\sigma^* t - i l \theta} \right) e^{-i \mu_2 t + i S_2 \theta},\end{aligned}\tag{31}$$

where l is an integer azimuthal index of the perturbation with components $u_{1,2}$, $v_{1,2}$, and σ is the instability growth rate.

Linearization around the stationary solutions leads to the BdG equations for the two-component condensate:

$$\begin{aligned}-\frac{1}{2} \left(u_1'' + \frac{1}{r} u_1' - \frac{(S+l)^2}{r^2} u_1 \right) + g_1 \Phi^2 (2u_1 + u_2) + g_{12} \Psi^2 u_1 + g_{12} \Psi \Phi (v_1 + v_2) - \mu_1 u_1 &= i \sigma u_1, \\ -\frac{1}{2} \left(u_2'' + \frac{1}{r} u_2' - \frac{(S-l)^2}{r^2} u_2 \right) + g_1 \Phi^2 (2u_2 + u_1) + g_{12} \Psi^2 u_2 + g_{12} \Psi \Phi (v_1 + v_2) - \mu_1 u_2 &= -i \sigma u_2, \\ -\frac{1}{2} \left(v_1'' + \frac{1}{r} v_1' - \frac{(S+l)^2}{r^2} v_1 \right) + g_2 \Psi^2 (2v_1 + v_2) + g_{12} \Phi^2 u_1 + g_{12} \Psi \Phi (u_1 + u_2) - \mu_2 v_1 &= i \sigma v_1, \\ -\frac{1}{2} \left(v_2'' + \frac{1}{r} v_2' - \frac{(S-l)^2}{r^2} v_2 \right) + g_2 \Psi^2 (2v_2 + v_1) + g_{12} \Phi^2 u_2 + g_{12} \Psi \Phi (u_1 + u_2) - \mu_2 v_2 &= -i \sigma v_2,\end{aligned}\tag{32}$$

where the prime stands for d/dr . Instabilities are predicted when numerical solution of Eq. (32) produces eigenvalues with $\text{Re}(\sigma) \neq 0$. In the 1D version of Eq. (32), d^2/dr^2 is replaced by d^2/dx^2 , and terms $\sim 1/r$ and $1/r^2$ are absent.

Previously, BdG equations were addressed in the annular geometry defined not by the rigid boundaries, as per Eq. (2), but by weak confinement constructed as the sum of Gaussian and harmonic oscillator potentials [67]. BdG equations for two-component condensates were also studied in other settings, including free space [88, 89], 1D configurations [62], and a full analytical solution [64].

III. RESULTS AND DISCUSSION

A. The one-dimensional regime

Stationary solutions to Eqs.(1) were produced numerically by means of the imaginary-time-evolution method, using different inputs. Then, stability of these solutions was identified through the calculation of their eigenvalue spectra, using the 1D version of Eq. (32), and further verified by direct numerical simulations of the perturbed evolution. The system conserves the total norm, i.e., scaled number of atoms. $N_{\text{total}} = N_\phi + N_\psi \equiv \int_0^{2\pi} (|\phi|^2 + |\psi|^2) dx$. Below, we report numerical results obtained for the basic symmetric states, with $m_1 = m_2 = 1$ (fixed by scaling), $g_1 = g_2 \equiv g$, $g_{12} = 1$ [also fixed by scaling, cf. Eq. (20)] and equal 1D norms in the two components,

$$\int_0^{2\pi} |\phi(x)|^2 dx = \int_0^{2\pi} |\psi(x)|^2 dx \equiv N.\tag{33}$$

In the miscible phase, the two components of the condensates overlap with each other, whereas they spatially separate in the immiscible phase. A measure to characterize these phases is the overlap integral Λ :

$$\Lambda = \frac{[\int \int dxdy |\phi(x, y)|^2 |\psi(x, y)|^2]^2}{[\int \int dxdy |\phi(x, y)|^4] [\int \int dxdy |\psi(x, y)|^4]}.\tag{34}$$

In this work, we identified demixed and mixed states as those with $\Lambda \neq 1$ and $\Lambda = 1$, respectively.

As expected [84, 90], demixed states exist only when the cross-repulsion is stronger than the self-repulsion, i.e., $g \leq g_{12} = 1$. They are characterized by local density peaks in each component, located so that a peak in one component coincides with a density minimum in the other, see insets to Figs. 2(b)-(d). Overlap integral (34) for 1D single-peak demixed modes is displayed in Fig. 2(a), as a function of self-repulsive coefficient g , for a fixed norm, $N = 10$. In this figure, the demixed single-peak mode terminates at $g_{\text{cr}} = 0.845$, only the uniformly mixed state existing at $g > g_{\text{cr}}$. This numerically identified critical value *exactly coincides with* the analytical prediction given by Eq. (18). Further, the existence area for demixed single-peak and mixed modes is presented in Fig. 2(b).

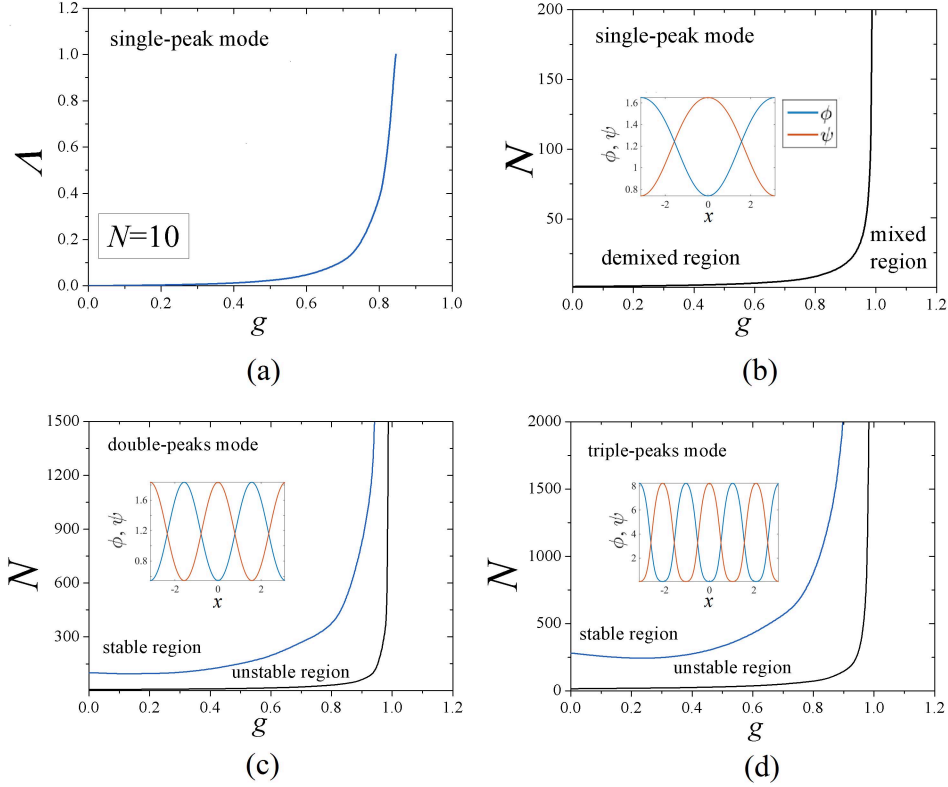


FIG. 2: (Color online) Numerically generated existence and stability areas for 1D mixed and demixed modes: (a) Overlap integral Λ of the ϕ and ψ components, defined as per Eq. (34), versus self-repulsion coefficient g , for single-peak modes with fixed norm $N = 10$, see Eq. (33); recall that the inter-species repulsion coefficient is fixed to be $g_{12} = 1$. Stability and existence areas for the single-peak, double-peaks, and triple-peak modes in the plane of (g, N) are displayed, respectively, in panels (b), (c), and (d). Black bottom curves in (b), (c) and (d) separate demixed (left) and mixed (right) states, while blue curves in (c) and (d) separate stable and unstable demixed ones. Insets in panels (b), (c) and (d) represent, respectively, typical examples of a stable single-peak mode [with parameters $(N, g, \Lambda) = (10, 0.8, 0.37)$], unstable double-peak one [for $(N, g, \Lambda) = (10, 0.1, 0.14)$], and unstable triple-peak state, for $(N, g, \Lambda) = (150, 0.1, 6.34 \times 10^{-4})$.

The boundary between them, analytically predicted by Eq. (18), also exactly coincides with the numerically found counterpart, shown by the black curve in Fig. 2(b). The single-peak demixed modes are completely stable in their existence domain, which is consistent with earlier findings [68].

Stability and existence areas of demixed double- and triple-peak modes are displayed in parameter plane (g, N) in Figs. 2(c) and (d), respectively, and typical examples of such modes are displayed in their respective insets. An essential finding is that, unlike the single-peak modes which are always stable, states with two and three peaks feature instability areas in Figs. 2(c) and (d), being stable only for a sufficiently large norm.

The numerical analysis reveals two instability scenarios for the double-peak mode. If it is taken in the area far from the stability boundary in Fig. 2(c), the real parts of the corresponding eigenvalues σ are relatively large [see Eq. (31)], and the mode spontaneously transforms into an oscillating single-peak state, see Fig. 3(a1-a3). If the unstable mode is selected close to the instability boundary, with smaller real parts of the eigenvalues, it oscillates around itself, rather than transforming into a single-peak state. Similar to the double-peak states, unstable triple-peak ones transform into oscillating single-peaks modes far from the corresponding stability boundary, and persistently oscillate around themselves, if taken close to boundary, see Fig. 3(b1-b3).

We also simulated collision between single-peak demixed components, set in motion by applying opposite kicks to them:

$$\phi(x, t = 0) = \phi(x)e^{ikx}, \quad \psi(x, t = 0) = \psi(x)e^{-ikx}. \quad (35)$$

Figure 4 shows that, for the kick small enough ($k = 0.5$), the peaks in the two components periodically bounce back from each other, which is accompanied by some randomization of the patterns. On the other hand, under the action of a strong kick (e.g., $k = 5$), the moving components pass through each other for about five times, but eventually

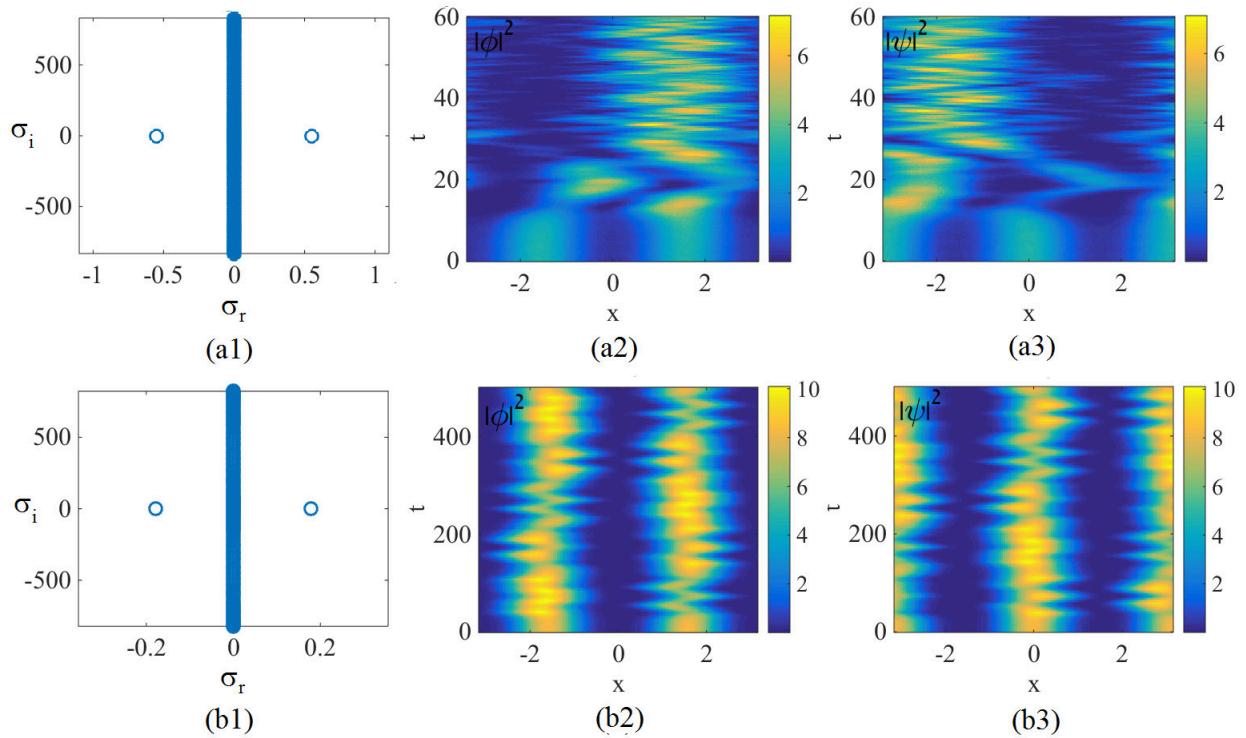


FIG. 3: (Color online) Eigenvalue spectra and direct simulations for two generic types of unstable 1D double-peaks modes. Panels (a1-a3), for the parameter set $(N, g, \Lambda) = (10, 0.1, 0.1354)$, taken far from the stability boundary, show the transformation into a persistent single-peak mode with irregular oscillations. Panels (b1-b3), for $(N, g, \Lambda) = (20, 0.1, 0.0104)$, show oscillations of the weakly unstable double-peak state around itself close to the instability boundary.

suffer randomization too, as shown in Fig. 4(b1,b2). Under the action of a still stronger kick, $k = 10$, the components kept passing through each as long as the simulations were run, see Fig. 4(c1,c2).

It is also relevant to simulate evolution of unstable mixed (uniform) states, which is displayed in Fig. 5. The instability triggers periodic transformations between the mixed state and a single-peak demixed one, with the period ≈ 10 in this case.

B. Two-dimensional regime

Focusing on the phase-separation scenarios, we identify two different types of 2D demixed modes, namely, those which may be defined as demixed in the radial direction (cf. Ref. [66]), and azimuthally demixed ones, cf. Refs. [62, 66, 67]. In previous works, similar scenarios of the phase separation were also reported for other binary systems, which include rotation [62, 68] and spin-orbit coupling [70].

1. Radially-demixed modes

In the consideration of the 2D setting subject to b.c. (2), we focus, as above, on the scaled symmetric system, with $m_1 = m_2 \equiv 1$, $g_1 = g_2 \equiv 1$, $g_{12} = 1$, and $r_{\text{inner}} = 1$, cf. Eqs. (20) and (3). Stability of 2D modes was identified by the computation of the eigenvalue spectra in the corresponding Bogoliubov-de Gennes (BdG) equations (32), and further verified by direct simulations.

First, we address 2D zero-vorticity states, including mixed and radially-demixed ones, which may be both stable and unstable (at larger and smaller values of the norm, respectively), as shown in Fig. 6. A typical example of the evolution of unstable 2D radially-demixed states with vorticities $S_{1,2} = 0$ is shown in Fig. 7. It is observed that the unstable state spontaneously evolves into an azimuthally-demixed one.

A noteworthy finding is that the system supports *stable* 2D radially-demixed states with *arbitrarily high* vorticities $S_1 = S_2 \equiv S$. We first analyze 2D demixed states with $S = 0$ and $S = 5$ in the parameter space of (g, N, Λ) , see Fig.

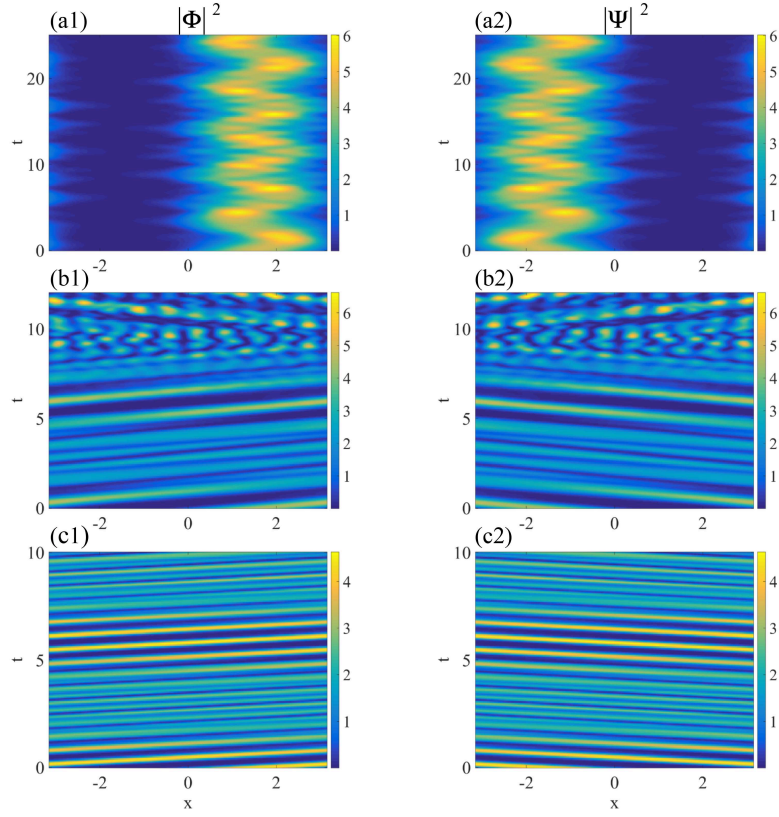


FIG. 4: (Color online) Collisions of between components of 1D single-peak modes, with parameters $(N, g, \Lambda) = (10, 0.1, 1.8 \times 10^{-3})$, initiated by kick (35) with $k = 0.5$ (a1, a2), $k = 5$ (b1, b2), and $k = 10$ (c1, c2).

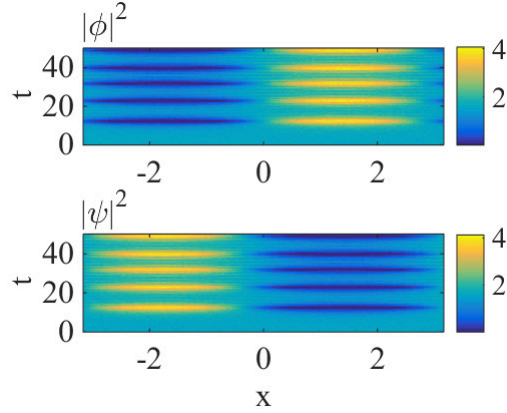


FIG. 5: (Color online) Numerically simulated evolution of an unstable 1D mixed mode, showing periodic transformations between mixed and demixed states. The parameters are $(N, g, \Lambda) = (10, 0.6, 1)$.

8. It is seen that the solutions are stable (similar to what was found above for other configurations) above a threshold value of the norm, $N > N_{\text{th}}$. We stress that the stability threshold is much lower for $S = 5$ than for $S = 0$ [note different scales of vertical axes in Figs. 8(a) and (b)].

To further explore how the vorticity affects the stability of the 2D demixed states, we define the atomic density,

$$n = \frac{N}{\pi(r_{\text{outer}}^2 - 1)} \quad (36)$$

[recall that the inner radius of the annulus is scaled to be 1, as per Eq. (3)], and display the stability-threshold value of n as a function of S in Fig. 9(a). A salient feature is the steep drop of n_{th} while S increases from 1 to 2, which is

followed by gradual decrease of the threshold with further increase of N . Thus, the vorticity helps to strongly stabilize the axially symmetric states in the annular domain.

It is also relevant to investigate an effect of the annulus' width w , defined as per Eq. (4), on the stability. For the zero-vorticity radially-demixed states, the respective stability diagram in parameter panel (n, w) is presented in Fig. 9(b)). It is seen that the stability area strongly broadens with the increase of w , i.e., as it might be expected, stable radially-demixed modes prefer broad annular domains.

2. Azimuthally-demixed modes (with $S = 0$)

The 2D setting supports, as well, stable modes which are phase-separated in the azimuthal direction (with zero vorticity) [68, 70], an example of such modes can be seen in Fig. 10. These modes are related to their 1D counterparts displayed above in the insets of Figs. 2(b,c,d), and unstable 2D radially-demixed modes transform into them (in an excited oscillating state), see Fig. 7.

To illustrate the evolution of those 2D azimuthally-demixed states which are unstable, we display the evolution of an unstable double-peak state with a small total norm, $N = 20$ in Fig.11 (similar to other states considered here, they tend to be unstable for relatively small values of N). It first evolves into a pattern with unequal heights of two peaks, and then restored the original configuration with equal peaks. After several cycles of such shape oscillations, it finally settles into an oscillating single-peak state. The same happens with unstable triple-peak 2D states. This kind of dynamics resembles what was observed above for unstable double- and triple-peak states in the 1D geometry, see Fig. 3.

On the other hand, we have not found any azimuthally-demixed states with nonzero vorticity.

Finally, it makes sense to address demixed modes in the full circle, with $r_{\text{inner}} = 0$, instead of the annulus, cf. Eq. (3). It has been found that radially-demixed modes may (quite naturally) exist in the latter case, while no azimuthally-demixed states were found.

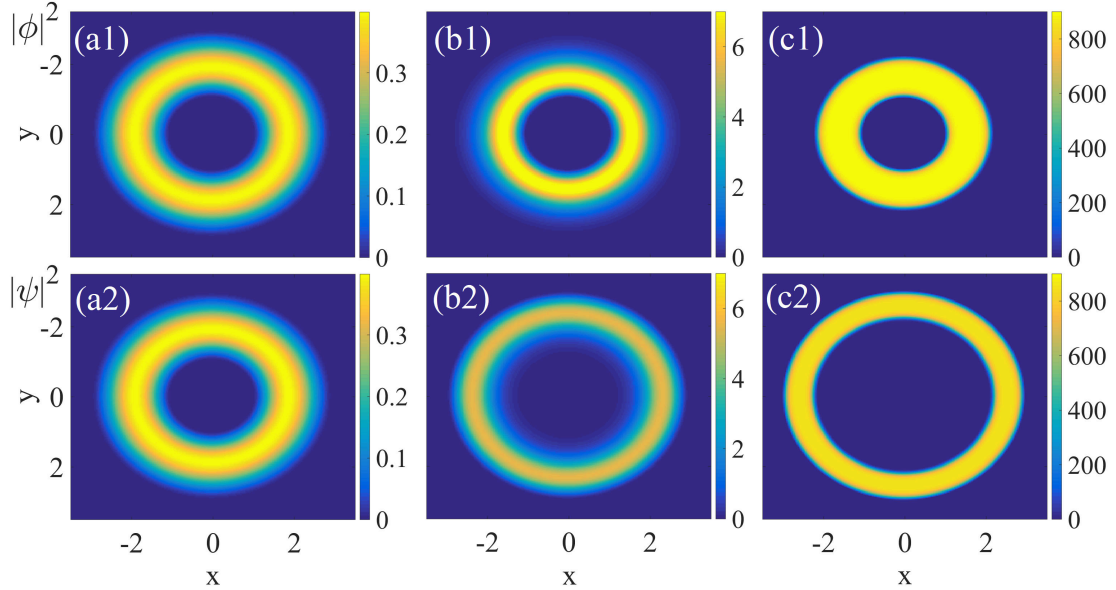


FIG. 6: (Color online) Typical examples of 2D zero-vorticity states ($S_{1,2} = 0$) with $g = 0.1$ and width $w = 2$. (a1,a2): An unstable mixed state with $N = 5$ and $\Lambda = 1$; (b1,b2): an unstable demixed state with $N = 60$ and overlap parameter $\Lambda = 0.1307$ [see Eq. (34)]; (c1,c2): a stable strongly demixed state with $N = 9000$ and $\Lambda = 4.45 \times 10^{-6}$.

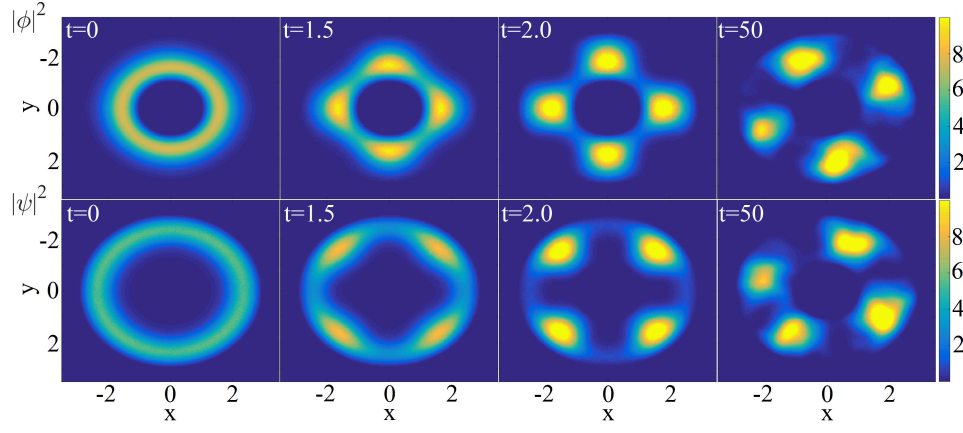


FIG. 7: (Color online) Density snapshots of the evolution of an unstable 2D radially-demixed mode shown in Fig. 6 (middle), revealing spontaneous formation of azimuthally-demixed states.

C. Hidden-vorticity states

1. The 1D setting

A typical example of the HV state, predicted by analytical solution (12), is presented in Fig. 12. This particular HV state is an unstable one, as illustrated in Fig. 1(a) by the dependence of its instability growth rate on the perturbation wavenumber, which is predicted by Eq. (22); for comparison, Fig. 1 (b) exhibits the same analytical result for a stable HV state. Simulations demonstrate that the evolution transforms unstable 1D HVs into stable single-peak demixed states, with some intrinsic oscillations (not shown here in detail).

2. The 2D setting

We have also numerically produced 2D radially-demixed HV states, example of which, with $S_{1,2} = \pm 1$ and ± 5 , are displayed in Figs. 13(a) and (b), respectively. The same setting may also support 2D mixed HV states, which we do not consider here in detail, as the demixed states seem more interesting. Results for the stability of the 2D radially-demixed HV modes with the same values of $S_{1,2}$ are summarized in Figs. 13(c) and (d). An obviously interesting

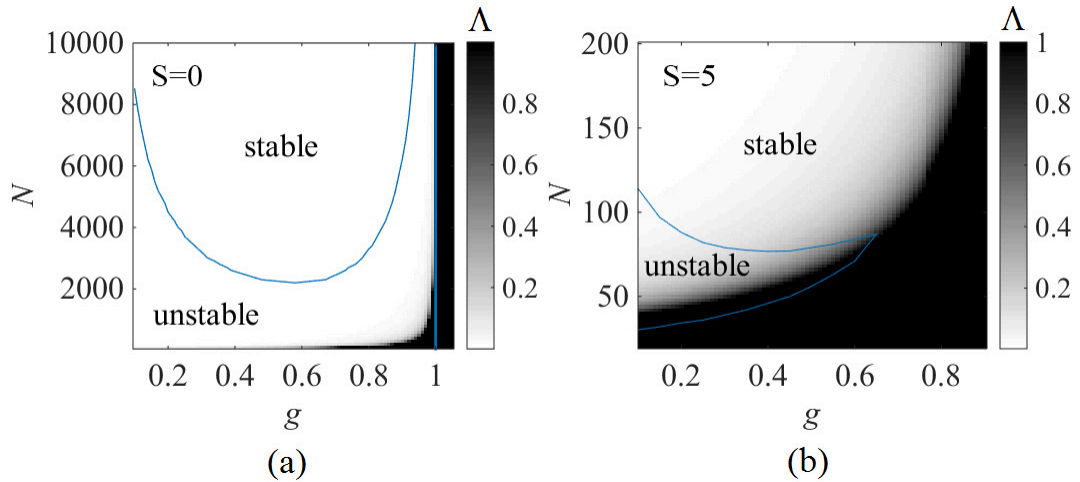


FIG. 8: (Color online) Existence and stability areas in the (g, N) plane for 2D mixed and radially-demixed states, in the annular domain with width $w = 2$ [see Eq. (4)]. The overall vorticity is $S = 0$ in (b1) and $S = 5$ in (b2). The gray-scaled shading shows the corresponding values of the overlap parameter Λ , see Eq. (34).

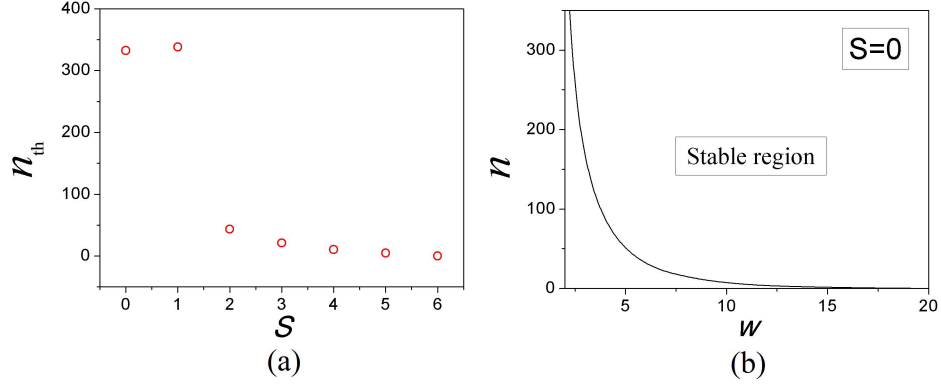


FIG. 9: (Color online) (a) The threshold value of density (36) of 2D radially-demixed states versus their vorticity S , the solutions being stable at $n \geq n_{\text{th}}$. The corresponding parameter set is $(w, g) = (2, 0.1)$, see Eqs. (20) and (4). (b) The stability region for the radially-demixed state with $S = 0$ in the plane of plane (n, w) , for $g = 0.1$. The solutions are stable above the solid curve.

conclusion following from the latter plots is that the increase of the hidden vorticity, $|S_{1,2}|$, leads to *stabilization* of the the HV states [note that difference in the scales of vertical axes in panels (c) and (d)].

Finally, comparing the total energy of different 2D mixed and demixed states [see Eq. (6)], which share equal values of the total norm and angular momentum, we have concluded that the single-peak azimuthally-demixed states realize the lowest energy, i.e., the system's ground state, while the totally mixed configuration has the highest energy.

D. Physical Estimates

To translate the scaled units into the physical ones, we consider the binary condensate of ^{87}Rb atoms in two different spin states, such as ones with $F = 1, m_F = 1$ and $F = 1, m_F = 0$, and use the same parameters as experiments performed with the two-components condensate in a ring [71], with the radius $\lesssim 12 \mu\text{m}$, and the scattering length $a_s \sim 10 \text{ nm}$ [91]. We conclude that the stable effectively 1D modes predicted by the present analysis may have the actual transverse thickness $\sim 3 \mu\text{m}$, containing up to $\sim 10^4$ atoms, while the stable 2D modes, predicted for the same outer radius, $\lesssim 12 \mu\text{m}$, and the inner one $\lesssim 4 \mu\text{m}$, contain $10^4 \sim 10^5$ atoms.

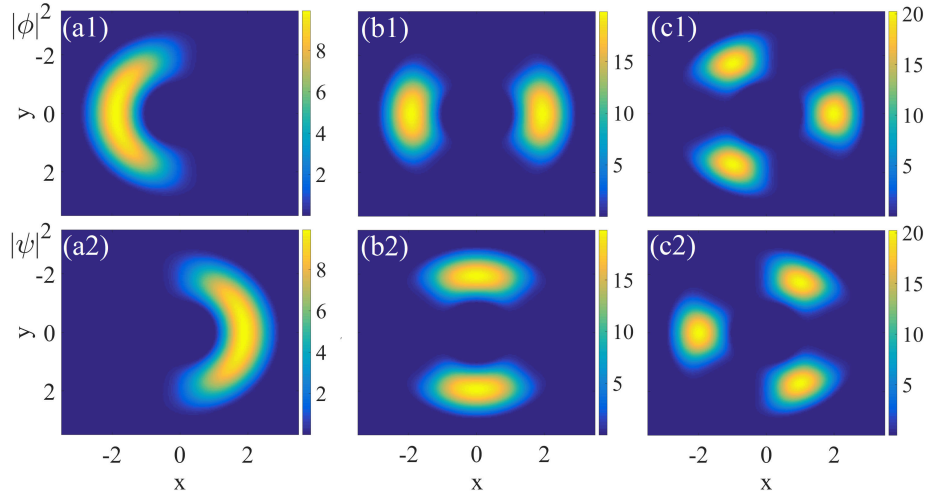


FIG. 10: (Color online) Typical examples of 2D azimuthally-demixed modes with zero vorticity, for $g = 0.1$ and the annulus' width $w = 2$. (a1,a2) A stable single-peak mode with total norm $N = 50$. (b1,b2) A stable double-peak mode with $N = 100$. (c1,c2) An unstable triple-peak mode with $N = 100$.

IV. CONCLUSION

We have studied the stability and phase diagram of the two-component BEC loaded in the 2D annular potential box, as well as its 1D limit form corresponding to a ring. The system was analyzed in the framework of the mean-field approximation, based on coupled Gross-Pitaevskii equations with repulsive intra-species and inter-species interactions.

In the 1D setting, the demixed (phase-separated) states are identified as single-, double- and triple-peak modes, with density peaks in one component coinciding with density minima in the other one. The 1D single-peak demixed states are all stable, while the double- and triple-peak ones are stable only above critical values of the total norm, N . The unstable double- and triple-peak modes oscillate around themselves when they are located close to the instability boundary, or spontaneously transform into stable single-peak states deeper in the unstable domain of the parameter space. Collisions between two components of stable demixed single-peak states were studied too, by applying opposite kicks to the components. The simulations demonstrate that the weakly kicked components repeatedly bounce from each other, suffering gradual chaotization, while fast ones pass through each other. If the kicks are moderately strong, the components originally pass through each other, and then evolve into the bouncing regime. The evolution of unstable 1D mixed (spatially uniform) modes shows periodic transitions between the mixed state and single-peak demixed ones.

In the 2D setting, we have found both radially- and azimuthally-demixed states, with unstable radially-demixed ones found to evolve into their azimuthally-demixed counterparts. An essential finding is that the system supports radially-demixed modes with arbitrarily large overall vorticity S , which are stable above the threshold value of the norm, N_{th} . The increase of S leads to stabilization of the modes (decrease of N_{th}), with a dramatic drop, following the transition from $S = 1$ to $S = 2$, in Fig. 9(a). The stability area gradually broadens with the increasing of the annulus' width, w , in Fig. 9(b). Similar to the 1D demixed states, 2D azimuthally-demixed ones are also identified as single-, double- and triple-peak modes. Unstable 2D double- and triple-peak azimuthally-demixed states (those with relatively small norms) evolve into oscillating single-peak modes. In the solid circle, taken instead of the annulus, only radially-demixed modes are found.

Lastly, both 1D and 2D HV (hidden-vorticity) states, with opposite vorticities in the two components, have been addressed too. The stability region for 1D HV modes was found analytically, and fully confirmed by the numerical analysis. Unstable 1D HV modes with components vorticities $S_{1,2} = \pm 1$ showed evolve into oscillating single-peak demixed modes. The stability domain for 2D radially-demixed HV modes expands with the increase of the hidden vorticity, $|S_{1,2}|$.

Acknowledgments

This work was supported, in part, by grants No.11874112 and No.11575063 from NNSFC (China), by grant No. 2015616 from the joint program in physics between NSF and Binational (US-Israel) Science Foundation, and by grant No. 1286/17 from the Israel Science Foundation. Z.C. acknowledges an excellence scholarship provided by the Tel Aviv University. B.A.M. appreciates hospitality of the Joint Quantum Centre (JQC) Durham-Newcastle, during his

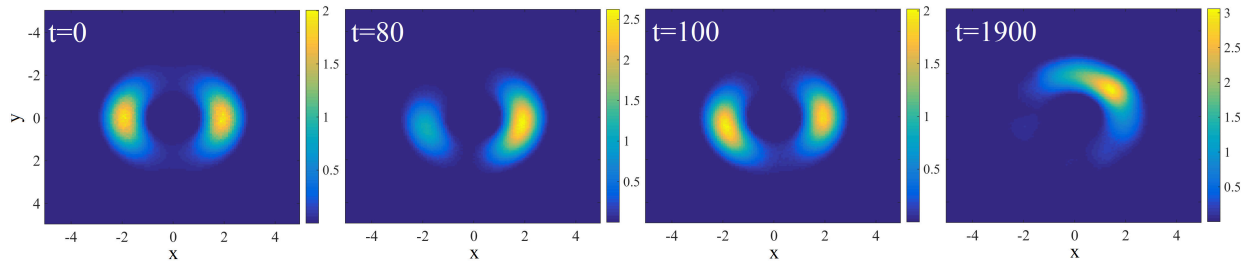


FIG. 11: (Color online) Density snapshots of the evolution of an unstable 2D double-peak azimuthally-demixed mode (only the $|\phi|^2$ component is displayed, as the complementary evolution of $|\psi|^2$ is similar) for $(g, w, N) = (0.1, 2, 20)$. The unstable mode spontaneously transforms into a stable single-peak one.

Visiting Professorship at Newcastle University, and NPP funding from EPSRC, UK (Grant No. EP/K03250X/1).

-
- [1] Myatt C J, Burt E A, Ghrist R W, Cornell E A and Wieman C E 1997 *Phys. Rev. Lett.* **78**(4) 586
 - [2] Hall D S, Matthews M R, Ensher J R, Wieman C E and Cornell E A 1998 *Phys. Rev. Lett.* **81**(8) 1539
 - [3] Maddaloni P, Modugno M, Fort C, Minardi F and Inguscio M 2000 *Phys. Rev. Lett.* **85**(12) 2413
 - [4] Mertes K M, Merrill J W, Carretero-González R, Frantzeskakis D J, Kevrekidis P G and Hall D S 2007 *Phys. Rev. Lett.* **99**(19) 190402
 - [5] Papp S B, Pino J M and Wieman C E 2008 *Phys. Rev. Lett.* **101**(4) 040402
 - [6] Sugawa S, Yamazaki R, Taie S and Takahashi Y 2011 *Phys. Rev. A* **84**(1) 011610
 - [7] Modugno G, Modugno M, Riboli F, Roati G and Inguscio M 2002 *Phys. Rev. Lett.* **89**(19) 190404
 - [8] Thalhammer G, Barontini G, De Sarlo L, Catani J, Minardi F and Inguscio M 2008 *Phys. Rev. Lett.* **100**(21) 210402
 - [9] McCarron D J, Cho H W, Jenkin D L, Köppinger M P and Cornish S L 2011 *Phys. Rev. A* **84**(1) 011603
 - [10] Lercher A D, Takekoshi T, Debatin M, Schuster B, Rameshan R, Ferlaino F, Grimm R and Nägerl H C 2011 *Eur. Phys. J. D* **65**(1) 3
 - [11] Pasquiou B, Bayerle A, Tzanova S M, Stellmer S, Szczepkowski J, Parigger M, Grimm R and Schreck F 2013 *Phys. Rev. A* **88**(2) 023601
 - [12] Wacker L, Jørgensen N B, Birkmose D, Horchani R, Ertmer W, Klempt C, Winter N, Sherson J and Arlt J J 2015 *Phys. Rev. A* **92**(5) 053602
 - [13] Petrov D S 2015 *Phys. Rev. Lett.* **115**(15) 155302
 - [14] Wang F, Li X, Xiong D and Wang D 2016 *J. Phys. B: At., Mol. Opt. Phys.* **49** 015302
 - [15] Cabrera C R, Tanzi L, Sanz J, Naylor B, Thomas P, Cheiney P and Tarruell L 2018 *Science* **359** 301–304 ISSN 0036-8075 (Preprint <https://science.sciencemag.org/content/359/6373/301.full.pdf>)
 - [16] Cheiney P, Cabrera C R, Sanz J, Naylor B, Tanzi L and Tarruell L 2018 *Phys. Rev. Lett.* **120**(13) 135301
 - [17] Semeghini G, Ferioli G, Masi L, Mazzinghi C, Wolswijk L, Minardi F, Modugno M, Modugno G, Inguscio M and Fattori M 2018 *Phys. Rev. Lett.* **120**(23) 235301
 - [18] Ferioli G, Semeghini G, Masi L, Giusti G, Modugno G, Inguscio M, Gallemí A, Recati A and Fattori M 2019 *Phys. Rev. Lett.* **122**(9) 090401
 - [19] Stamper-Kurn D M and Ueda M 2013 *Rev. Mod. Phys.* **85**(3) 1191
 - [20] Galitski V and Spielman I B 2013 *Nature* **494** 49 EP –
 - [21] Zhou X, Li Y, Cai Z and Wu C 2013 *Journal of Physics B: Atomic, Molecular and Optical Physics* **46** 134001
 - [22] Goldman N, Juzeliūnas G, Høberg P and Spielman I B 2014 *Reports on Progress in Physics* **77** 026401
 - [23] Zhai H 2015 *Reports on Progress in Physics* **78** 026001
 - [24] Malomed B A 2018 *EPL (Europhysics Letters)* **122** 36001
 - [25] Ferrier-Barbut I, Delehaye M, Laurent S, Grier A T, Pierce M, Rem B S, Chevy F and Salomon C 2014 *Science* **345** 1035 ISSN 0036-8075
 - [26] Esry B D, Greene C H, Burke Jr J P and Bohn J L 1997 *Phys. Rev. Lett.* **78**(19) 3594–3597
 - [27] Pu H and Bigelow N P 1998 *Phys. Rev. Lett.* **80**(6) 1130–1133
 - [28] Ao P and Chui S T 1998 *Phys. Rev. A* **58**(6) 4836–4840
 - [29] Timmermans E 1998 *Phys. Rev. Lett.* **81**(26) 5718–5721
 - [30] Öhberg P 1999 *Phys. Rev. A* **59** 634
 - [31] Trippenbach M, Góral K, Rzazewski K, Malomed B and Band Y B 2000 *J. Phys. B: At. Mol. Opt. Phys.* **33** 4017
 - [32] Delannoy G, Murdoch S G, Boyer V, Josse V, Bouyer P and Aspect A 2001 *Phys. Rev. A* **63**(5) 051602
 - [33] Riboli F and Modugno M 2002 *Phys. Rev. A* **65**(6) 063614

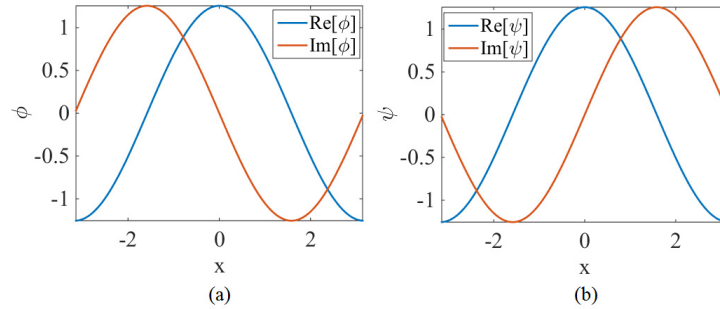


FIG. 12: (Color online) A typical example of an unstable one-dimensional HV (hidden-vorticity) mode with $(g, N, S_1, S_2) = (0.1, 10, -1, 1)$

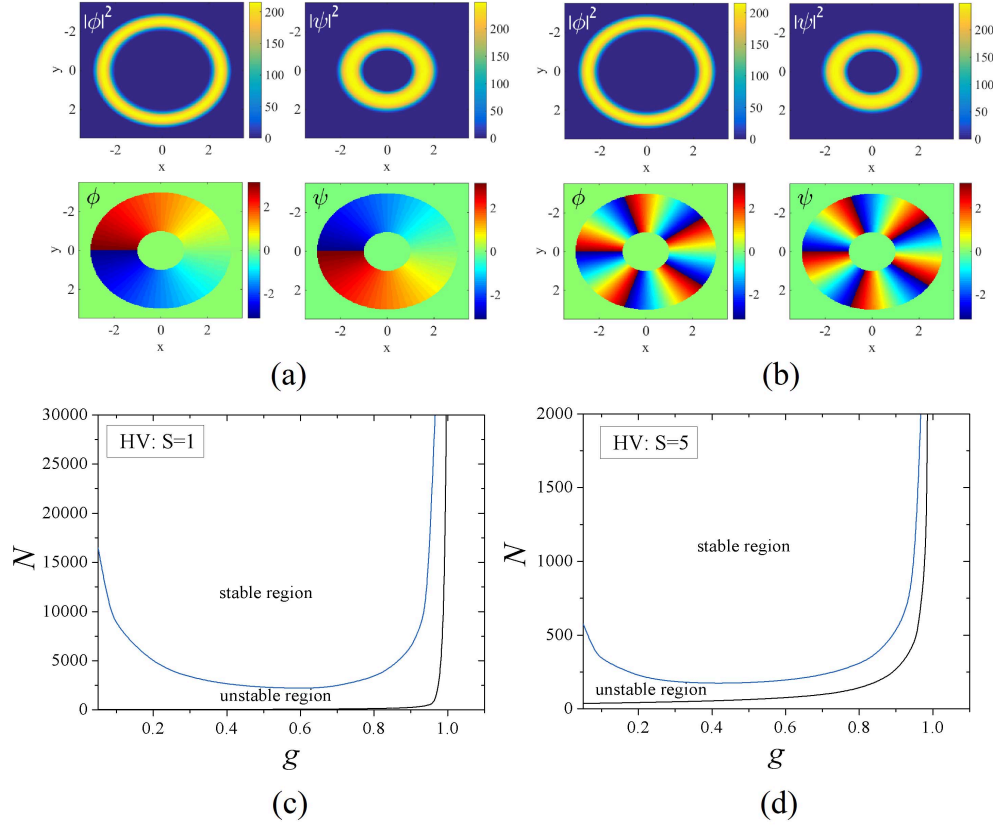


FIG. 13: (Color online) Typical examples (the density distribution and phase structure) of stable 2D radially-demixed HV states: (a) $S_{1,2} = \pm 1$; (b) $S_{1,2} = \pm 5$. Both examples correspond to the same parameter set, $(g_{1,2}, w \equiv r_{\text{outer}} - 1, N) = (0.1, 2, 2000)$. Panels (c) and (d) summarize properties of the respective HV states in parameter plane (g, N) . In (c) and (d), black curves separate demixed and mixed states (left and right areas, respectively), while blue curves are stability boundaries for demixed states.

- [34] Jezek D M and Capuzzi P 2002 *Phys. Rev. A* **66**(1) 015602
- [35] Svidzinsky A A and Chui S T 2003 *Phys. Rev. A* **68**(1) 013612
- [36] Kasamatsu K and Tsubota M 2004 *Phys. Rev. Lett.* **93**(10) 100402
- [37] Ronen S, Bohn J L, Halmo L E and Edwards M 2008 *Phys. Rev. A* **78**(5) 053613
- [38] Takeuchi H, Ishino S and Tsubota M 2010 *Phys. Rev. Lett.* **105**(20) 205301
- [39] Suzuki N, Takeuchi H, Kasamatsu K, Tsubota M and Saito H 2010 *Phys. Rev. A* **82**(6) 063604
- [40] Mason P and Aftalion A 2011 *Phys. Rev. A* **84**(3) 033611
- [41] Aftalion A, Mason P and Wei J 2012 *Phys. Rev. A* **85**(3) 033614
- [42] Wen L, Liu W M, Cai Y, Zhang J M and Hu J 2012 *Phys. Rev. A* **85**(4) 043602
- [43] Pattinson R W, Billam T P, Gardiner S A, McCarron D J, Cho H W, Cornish S L, Parker N G and Proukakis N P 2013 *Phys. Rev. A* **87**(1) 013625
- [44] Hofmann J, Natu S S and Das Sarma S 2014 *Phys. Rev. Lett.* **113**(9) 095702
- [45] Pattinson R W, Parker N G and Proukakis N P 2014 *J. Phys.: Conf. Ser.* **497** 012029
- [46] Edmonds M J, Lee K L and Proukakis N P 2015 *Phys. Rev. A* **91**(1) 011602
- [47] Edmonds M J, Lee K L and Proukakis N P 2015 *Phys. Rev. A* **92**(6) 063607
- [48] Lee K L and Proukakis N P 2016 *Journal of Physics B: Atomic, Molecular and Optical Physics* **49** 214003
- [49] Liu I K, Pattinson R W, Billam T P, Gardiner S A, Cornish S L, Huang T M, Lin W W, Gou S C, Parker N G and Proukakis N P 2016 *Phys. Rev. A* **93**(2) 023628
- [50] Lee K L, Jørgensen N B, Liu I K, Wacker L, Arlt J J and Proukakis N P 2016 *Phys. Rev. A* **94**(1) 013602
- [51] Lee K L, Jørgensen N B, Wacker L J, Skou M G, Skalmstang K T, Arlt J J and Proukakis N P 2018 *New Journal of Physics* **20** 053004
- [52] Li Y, Chen Z, Luo Z, Huang C, Tan H, Pang W and Malomed B A 2018 *Phys. Rev. A* **98**(6) 063602
- [53] Gupta S, Murch K W, Moore K L, Purdy T P and Stamper-Kurn D M 2005 *Phys. Rev. Lett.* **95**(14) 143201
- [54] Arnold A S, Garvie C S and Riis E 2006 *Phys. Rev. A* **73**(4) 041606
- [55] Ryu C, Andersen M F, Cladé P, Natarajan V, Helmerson K and Phillips W D 2007 *Phys. Rev. Lett.* **99**(26) 260401

- [56] Ramanathan A, Wright K C, Muniz S R, Zelan M, Hill W T, Lobb C J, Helmerson K, Phillips W D and Campbell G K 2011 *Phys. Rev. Lett.* **106**(13) 130401
- [57] Eckel S, Lee J G, Jendrzejewski F, Murray N, Clark C W, Lobb C J, Phillips W D, Edwards M and Campbell G K 2014 *Nature* **506** 200
- [58] Corman L, Chomaz L, Bienaimé T, Desbuquois R, Weitenberg C, Nascimbène S, Dalibard J and Beugnon J 2014 *Phys. Rev. Lett.* **113**(13) 135302
- [59] Kumar A, Eckel S, Jendrzejewski F and Campbell G K 2017 *Phys. Rev. A* **95**(2) 021602
- [60] Amico L, Birkel G, Boshier M and Kwek L C 2017 *New Journal of Physics* **19** 020201
- [61] Smyrnakis J, Bargi S, Kavoulakis G M, Magiropoulos M, Kärkkäinen K and Reimann S M 2009 *Phys. Rev. Lett.* **103**(10) 100404
- [62] Shimodaira T, Kishimoto T and Saito H 2010 *Phys. Rev. A* **82**(1) 013647
- [63] Bargi S, Malet F, Kavoulakis G M and Reimann S M 2010 *Phys. Rev. A* **82**(4) 043631
- [64] Anoshkin K, Wu Z and Zaremba E 2013 *Phys. Rev. A* **88**(1) 013609
- [65] Yakimenko A I, Isaieva K O, Vilchinskii S I and Weyrauch M 2013 *Phys. Rev. A* **88**(5) 051602
- [66] Mason P 2013 *Eur. Phys. J B* **86** 453
- [67] Abad M, Sartori A, Finazzi S and Recati A 2014 *Phys. Rev. A* **89**(5) 053602
- [68] White A, Hennessy T and Busch T 2016 *Phys. Rev. A* **93**(3) 033601
- [69] Yakimenko A I, Bidasyuk Y M, Weyrauch M, Kuriatnikov Y I and Vilchinskii S I 2015 *Phys. Rev. A* **91**(3) 033607
- [70] White A C, Zhang Y and Busch T 2017 *Phys. Rev. A* **95**(4) 041604
- [71] Beattie S, Moulder S, Fletcher R J and Hadzibabic Z 2013 *Phys. Rev. Lett.* **110**(2) 025301
- [72] Desyatnikov A S and Kivshar Y S 2001 *Phys. Rev. Lett.* **87**(3) 033901
- [73] Desyatnikov A S, Mihalache D, Mazilu D, Malomed B A, Denz C and Lederer F 2005 *Phys. Rev. E* **71**(2) 026615
- [74] Bigelow M S, Park Q H and Boyd R W 2002 *Phys. Rev. E* **66**(4) 046631
- [75] Leykam D, Malomed B and Desyatnikov A S 2013 *Journal of Optics* **15** 044016
- [76] Salgueiro J R 2016 *Journal of Optics* **18** 074004
- [77] Mihalache D, Mazilu D, Lederer F, Kartashov Y V, Crasovan L C, Torner L and Malomed B A 2006 *Phys. Rev. Lett.* **97**(7) 073904
- [78] Brtko M, Gammal A and Malomed B A 2010 *Phys. Rev. A* **82**(5) 053610
- [79] Yakimenko A I, Shchebetovska K O, Vilchinskii S I and Weyrauch M 2012 *Phys. Rev. A* **85**(5) 053640
- [80] He J R, Li H M and Li L 2012 *Physics Letters A* **376** 3108 – 3112 ISSN 0375-9601
- [81] Wen L, Qiao Y, Xu Y and Mao L 2013 *Phys. Rev. A* **87**(3) 033604
- [82] Ishino S, Tsubota M and Takeuchi H 2013 *Phys. Rev. A* **88**(6) 063617
- [83] Hoashi M, Nakamura Y and Yamanaka Y 2016 *Phys. Rev. A* **93**(4) 043622
- [84] Mineev V *Zh. Eksp. Teor. Fiz., v. 67, no. 1, pp. 263-272*
- [85] Merhasin I M, Malomed B A and Driben R 2005 *Physica Scripta* **18**
- [86] Hueck K, Luick N, Sobirey L, Siegl J, Lompe T and Moritz H 2018 *Phys. Rev. Lett.* **120**(6) 060402
- [87] Dodd R J 1996 *Journal of research of the National Institute of Standards and Technology* **101** 545–552
- [88] Ishino S, Tsubota M and Takeuchi H 2011 *Phys. Rev. A* **83**(6) 063602
- [89] Law C K, Chan C M, Leung P T and Chu M C 2001 *Phys. Rev. A* **63**(6) 063612
- [90] Lingua F, Guglielmino M, Penna V and Capogrosso Sansone B 2015 *Phys. Rev. A* **92**(5) 053610
- [91] Egorov M, Opanchuk B, Drummond P, Hall B V, Hannaford P and Sidorov A I 2013 *Phys. Rev. A* **87**(5) 053614